Journal of Materials Chemistry C

PAPER

View Article Online
View Journal | View Issue

Cite this: J. Mater. Chem. C, 2015, 3, 9670

Enhancing the performance of polymer solar cells by tuning the drying process of blend films *via* changing side chains and using solvent additives†

Jicheng Zhang, Xuejuan Zhang, Guangwu Li, Wenhua li,* Chong Kang, Xiuxiu Zhao, Heng Lu and Zhishan Bo*

Received 16th June 2015,
Accepted 23rd August 2015

DOI: 10.1039/c5tc01788b

www.rsc.org/MaterialsC

A series of new conjugated polymers (**P1–P3**) with 3,6-difluorocarbazole as a donor unit and benzoxadiazole as an acceptor unit were synthesized and used as donor materials for polymer solar cells (PSCs). The morphology of blend films was regulated by controlling the drying process *via* tuning the solubility of polymers and using solvent additives. Enhancing the solubility of polymers *via* increasing the volume of side chains can decrease the domain size of polymers and using 1,8-diiodooctane (DIO) as a solvent additive can give an even better vertical phase separation, leading to a significant enhancement of the power conversion efficiency (PCE) of up to 5.71% for **P3** based PSCs. The improving of the interface between polymers and $PC_{71}BM$ phases as well as the formation of vertical phase separation after using DIO as an additive are probably responsible for the high open circuit voltage (V_{oc}) of devices.

Introduction

In the last two decades, bulk heterojunction polymer solar cells (BHJ PSCs) with conjugated polymers as donors and $PC_{71}BM$ as an acceptor have attracted particular attention because of their advantages of lightweight, low-cost and mechanical flexibility.[1–3] Significant progress has been made in recent years and power conversion efficiency (PCE) over 10% has been achieved.[4–8] These accomplishments were mostly driven by the design and synthesis of newly conjugated polymer materials, the optimization of devices and the investigation of the relationship between the chemical structure of polymers and the photovoltaic performance of devices.

Development of effective methods to tune the morphology of the BHJ layer is a significant task to improve device performance[9] and the solubility of polymers is very important to afford appropriate phase separation when blending with $PC_{71}BM$.[10] The morphology of the active layer is significantly influenced by the solubility of conjugated polymers. Generally, bad solubility of polymers usually causes oversized domains while evaporating from the solution which goes against the effective dissociation of the exciton. But good solubility, which comes from longer chains, usually affects the stacking of polymers as films. Therefore, using appropriate side chains to balance the solubility and planarity of conjugated polymers is beneficial to achieve best photovoltaic performance. Active layers with an appropriate vertical phase separation are beneficial to afford high performance of PSCs.[11] Conventional devices with a polymer rich bottom surface could enhance the collection of holes by the anode and suppress the bulk and interfacial bimolecular charge recombination. Such vertical phase separation of active layers could be optimized by adding DIO as an additive.[12]

Fluorine has been proved to be a good substituendum for acceptor groups of donor–acceptor (D–A) alternating polymers, the introduction of F atoms onto acceptor unit could significantly improve the photovoltaic performance of polymers,[13,14] but the introduction of F atoms onto donor positions may result in a different influence on the photovoltaic performance.[15,16] Since F atoms exhibit greatly positive effects in the improvement of the photovoltaic performance, extending the study of D–A conjugated polymers with a fluorinated donor unit is still of great significance to achieve higher efficiency photovoltaic polymers. Benzoxadiazole (BO) has been proved to be a good acceptor unit for the construction of D–A conjugated polymers used for PSCs.[17] Compared with the commonly used benzothiadiazole (BT) acceptor unit, BO could furnish deeper HOMO level for the resulted polymers. However, due to the high polarity of O atoms and the high planarity of the BO part, BO based polymers exhibited poor solubility.[18] By changing the side chains of conjugated backbones, **P1**, **P2** and **P3** with fluorinated carbazole as a donor unit, BO as an acceptor unit, and thiophene as a π bridge were

Beijing Key Laboratory of Energy Conversion and Storage Materials, College of Chemistry, Beijing Normal University, Beijing 100875, China. E-mail: liwenhua@bnu.edu.cn, zsbo@bnu.edu.cn

† Electronic supplementary information (ESI) available: Experimental part including TGA curves, SCLC curves, and ^{1}H NMR spectra of monomers and polymers. See DOI: 10.1039/c5tc01788b

synthesized in this work. All three polymers exhibited worse solubility compared with $PC_{71}BM$, which would lead to a liquid–solid mechanism in the film drying procedure.[19] But too bad solubility would cause oversized domains in the process of film drying. By gradually extending the side chains for **P1**, **P2** and **P3**, better solubility and higher hole mobility could be achieved, besides that the root-mean-square (RMS) roughness value of the film surface and series resistance values of devices all gradually reduced, which would lead to a higher PCE. XPS experiment demonstrated that **P1–3** were all donor rich in the bottom surface, which is beneficial for the hole injection by the electrode. Using DIO as an additive, the fluorescence intensity of polymers was decreased, indicating that the domain size of polymers became smaller. Besides that, hole mobility values of devices were further enhanced, series resistor values of the devices were further reduced, and the RMS roughness values of the active layers were decreased, which demonstrated that DIO could optimize the film morphology. The X-ray photoelectron spectroscopy (XPS) experiment also demonstrated that the contents of **P1–3** in the bottom surface were all enhanced with DIO as an additive, which would lead to better photovoltaic performance. Compared with the non-fluorinated polymer, fluorinated polymers exhibited lower HOMO levels, and open circuit voltage (V_{oc}), short circuit current (J_{sc}) and the fill factor (FF) were all improved to achieve higher PCE. Using 2% DIO as an additive, photovoltaic devices based on **P3** showed the best PCE of 5.71%.

Results and discussion

Material synthesis and characterization

The syntheses of monomers (**3a**, **3b**) and polymers (**P1**, **P2**, and **P3**) are outlined in Scheme 1. 2,7-Dibromo-3,6-difluoro-9*H*-carbazole(**1**),[20] 2,7-dibromo-3,6-difluoro-9-(2-hexyldecyl)-9*H*-carbazole (**2a**),[20] 4,7-bis(5-bromothiophen-2-yl)-5,6-dioctylbenzo[*c*][1,2,5]oxadiazole (**4a**),[21] 4,7-bis(5-bromothiophen-2-yl)-5,6-didodecylbenzo[*c*][1,2,5]oxadiazole (**4b**),[21] and 3,6-difluoro-9-(2-hexyldecyl)-2,7-bis(4,4,5,5-tetramethyl-1,3,2-dioxaborolan-2-yl)-9*H*-carbazole (**3a**)[20] were synthesized according to the literature procedures. **2b** was prepared in a yield of 82% by the reaction of compound **1** and 11-(bromomethyl)-tricosane in DMF with NaH as a base. The reaction of **2b** and bis(pinacolato)diboron by Miyaura reaction using $PdCl_2$(dppf) as a catalyst afforded **3b** in a yield of 62%. Suzuki polycondensation (SPC) of the dibromo monomers (**4a** and **4b**) with a diboronic acid ester monomer (**3a**) afforded polymers (**P1** and **P2**) as dark-red solids in yields of 70% and 78%, respectively. SPC of **3b** and **4b** furnished **P3** in a yield of 81% as a dark-red solid. SPCs were carried out in a biphasic mixture of THF/toluene (3 : 1) and aqueous $NaHCO_3$ with $Pd(PPh_3)_4$ as a catalyst precursor. After polymerization, the bromo and boronic acid end-groups were capped by phenylboronic acid and bromobenzene, respectively. The side chains have a great influence on the solubility of polymers and the solubility of polymers can be tuned by changing their side chains. **P1** carrying two octyloxy chains on the 5,6-positions of the benzothiadiazole unit and one 2-hexyldecyl chain on the 9-position of the 3,6-difluorocarbazole unit exhibited very poor solubility in chloroform (CF), chlorobenzene (CB), 1,2-dichlorobenzene (DCB), and 1,2,4-trichlorobenzene (TCB) at room temperature. Nevertheless, **P1** can be fully dissolved in DCB and TCB at temperature above 115 °C. **P2**, in which the two octyloxy chains on the 5,6-positions of the benzothiadiazole unit were changed to two dodecyloxy chains, exhibiting slightly better solubility than **P1**. **P2** is also almost insoluble in common organic solvents such as CF, CB, DCB, and TCB at room temperature, but can be fully soluble in CB, DCB, and TCB at temperature above 105 °C. **P3** with replacing the 2-hexyldecyl chain on the 9-position of 3,6-difluorocarbazole unit with 2-decyltetradecyl group showed further improved solubility in comparison with **P2**. **P3** is partially soluble in DCB and TCB at room temperature and can be fully dissolved in CB, DCB, and TCB at temperature above 80 °C. The molecular weights and polydispersity indexes (PDI) of **P1–3** measured by gel permeation chromatography (GPC) at 150 °C using TCB as an eluent and polystyrenes as the calibration standards are summarized in Table 1. Thermal stability of these polymers was investigated with thermogravimetric analysis (TGA) under a nitrogen atmosphere at a heating rate of 10 °C min^{-1}. **P1**, **P2**, and **P3** exhibited good thermal stability with 5% weight loss at 327 °C, 323 °C, and 318 °C, respectively, and the results are also summarized in Table 1. No glass transition temperature can be detected for **P1–3** by differential scanning calorimetry (DSC) in the range of 20 to 250 °C at a heating rate 10 °C min^{-1} under a nitrogen atmosphere. To investigate the packing of polymer chains in the solid state, powdery samples of **P1–3** were investigated by the X-ray diffraction (XRD) technique. As shown in Fig. 1, **P1** and **P2** present a relatively intense diffraction peak in the small angle region and a broad peak in the wide angle region, reflecting the lamella stacking and π–π stacking of polymers, respectively. The small angles of 4.51° for **P1** and 3.87° for **P2** revealed that

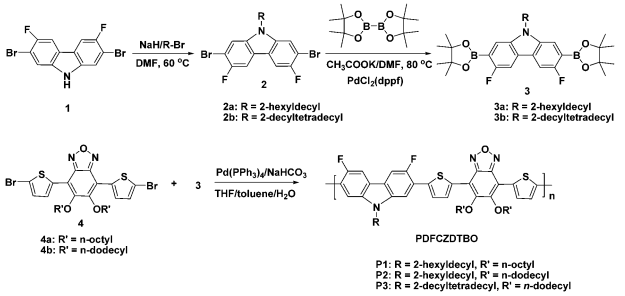

Scheme 1 Synthesis of monomers and polymers.

Table 1 M_n, M_w, PDI, and T_d of **P1–3**

Polymer	M_n[a] (kg mol^{-1})	M_w[a] (kg mol^{-1})	PDI	T_d[b] (°C)
P1	20.1	51.0	2.53	327
P2	22.1	58.1	2.63	323
P3	31.9	77.5	2.43	318

[a] M_n, M_w, and PDI were determined by GPC at 150 °C with TCB as an eluent calibrated with polystyrene standards. [b] T_d was determined by TGA under a N_2 atmosphere based on 5% weight loss.

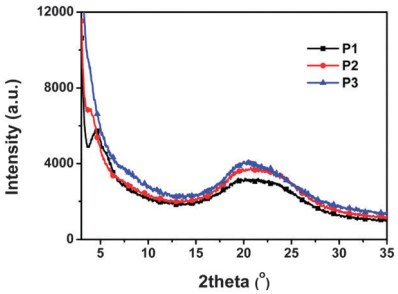

Fig. 1 XRD patterns of **P1–3** powders.

the stacking distances of polymer backbones separated by the flexible side chains are 19.58 Å for **P1** and 22.81 Å for **P2**. The diffraction peaks at 20.8°, 20.6° and 20.4° reflex the π–π stacking distances between the polymer backbones, which are calculated to be 4.28 Å, 4.31 Å and 4.33 Å for **P1**, **P2**, and **P3**, respectively. XRD investigations indicated that the π–π packing distance between polymer backbones can be slightly tuned by the side chains (Chart 1).

Optical properties

UV-vis absorption characteristics of **P1–3** in DCB (1×10^{-5} M) were investigated at an elevated temperature of 120 °C. As shown in Fig. 2a, all polymers exhibit three absorption peaks in the visible region. The peak located at around 386 nm can be attributed to the localized π–π* transition and the two peaks at a long wave length region can be ascribed to the internal charge transfer (ICT) interaction from the carbazole donor unit to the benzoxadiazole acceptor unit. The shoulder peak at about 573 nm can be attributed to the aggregation of polymer chains, and its intensity decreased slightly in the order of **P1**, **P2** and **P3** with the volume of side chains increasing gradually. UV-visible absorption spectra of **P1–3** films spin coated on quartz substrates are shown in Fig. 2b. On going from solution to film, the long wave length absorption peak red-shifted from 572 to 582 nm for **P1**, from 573 to 577 nm for **P2**, and from 573 to 574 nm for **P3**. This result indicates that larger side chains can weaken the interaction of polymers in the solid state. The film absorption onsets of **P1–3** are 632, 625, and 610 nm, corresponding to optical band gaps ($E_{g,opt}$) of 1.96, 2.00, and 2.03 eV, respectively. These data are also summarized in Table 2.

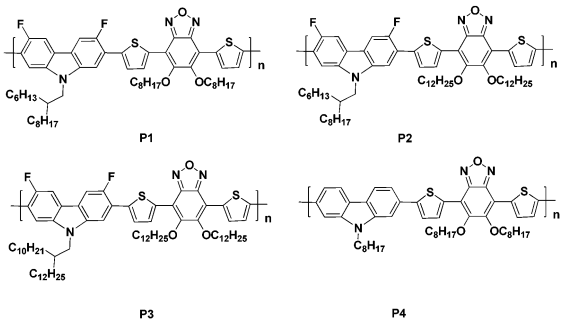

Chart 1

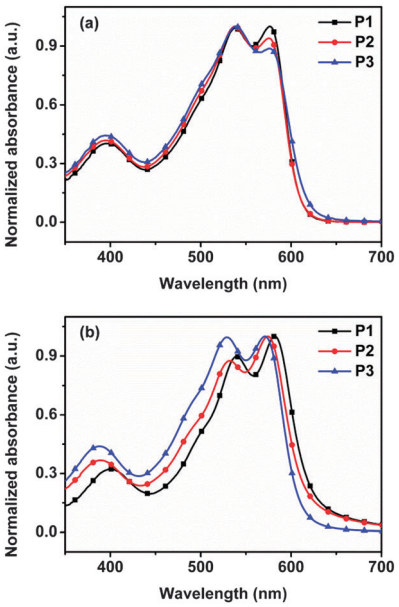

Fig. 2 UV-vis absorption spectra of **P1–3** in DCB solutions at 120 °C (a) and as thin films (b).

In comparison with the non-fluorinated polymer **P4**, the long wave length absorption peaks of **P1** and **P2** became much stronger, indicating that the introduction of F atoms into the donor unit can significantly enhance the interaction of polymers in the solid state. To investigate the influence of DIO as an additive on the aggregation of **P1–3** in the blend films, UV-visible absorption spectra of **P1–3**:$PC_{71}BM$ blend films with and without 2% DIO as an additive were also tested. As shown in Fig. S2 (ESI†), all films exhibited a broad absorption in the range from 350 nm to 650 nm. After using 2% DIO as an additive, the intensity of the peaks at around 550 nm all significantly decreased, demonstrating that using DIO as an additive could reduce the aggregation of **P1–3** in the blend film. To further investigate the influence of DIO as an additive on the charge recombination in the active layer, the fluorescence spectra of blend films also measured. As shown in Fig. S3 (ESI†), after using 2% DIO as an additive, the blend films all exhibited higher fluorescence quenching efficiencies. The enhancement of fluorescence quenching efficiency demonstrated using DIO as an additive could optimize the blend morphology and reduce the charge recombination in the blend films, which would lead to higher V_{oc} of devices.[22–27]

Table 2 Electronic and optical properties of **P1–4**

Polymer	λ_{max} (nm) solution	λ_{max} (nm) film	$E_{g,opt}$[a] (eV)	HOMO (eV)	LUMO[b] (opt, eV)
P1	387, 532, 572	400, 538, 582	1.96	−5.55	−3.59
P2	386, 532, 573	390, 535, 577	2.00	−5.57	−3.57
P3	385, 532, 573	389, 533, 574	2.03	−5.58	−3.55
P4[c]	—	385, 540	1.93	−5.34	−3.46

[a] Calculated from the absorption band edge of polymer films, $E_{g,opt} = 1240/\lambda_{edge}$. [b] Calculated by the equation $E_{LUMO} = E_{HOMO} + E_{g,opt}$. [c] Reference from literature.[19]

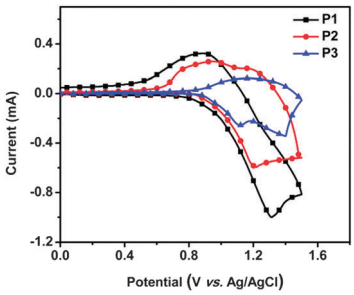

Fig. 3 Cyclic voltammograms of **P1–3** as thin films on a glassy carbon working electrode.

Electrochemical properties

Electrochemical properties of **P1–3** films were investigated by cyclic voltammetry on a glassy carbon working electrode. As shown in Fig. 3, the onset oxidation potentials (E_{ox}) of **P1–3** are 0.84, 0.86 and 0.87 eV *vs.* Ag/AgCl reference electrode. HOMO energy levels were determined according to the equation $E_{HOMO} = -e(E_{ox} + 4.71\ eV)$ to be −5.55 eV for **P1**, −5.57 eV for **P2**, and −5.58 eV for **P3**. LUMO levels of **P1**, **P2**, and **P3** were calculated by the equation $E_{LUMO} = E_{HOMO} + E_{g,opt}$ to be −3.59, −3.57, and −3.55 eV, respectively. The complete data are summarized in Table 2. The results indicated that increasing the volume of side chains has a subtle influence on electrochemical properties of polymers. Compared with the non-fluorinated **P4**, the presence of two F atoms on the carbazole donor unit lowers the HOMO levels of **P1–3** for about 0.2 eV. The fairly low-lying HOMO levels are beneficial to afford higher V_{oc} for PSCs.

Photovoltaic properties

To investigate the photovoltaic performance of **P1–3** as donor materials, devices with a configuration of ITO/PEDOT:PSS (40 nm)/**P1–3**:$PC_{71}BM$/LiF (0.5 nm)/Al (100 nm) were fabricated. Detailed studies on the processing solvent, the weight ratio of **P1–3** to $PC_{71}BM$, the concentration of blend solution, the spin-coating speed, the thickness of active layers, and the amount of 1,8-diiodooctane (DIO) additive were carried out to optimize the device performance. Since the poor solubility of **P1–3** in DCB at room temperature, all devices were fabricated by spin-coating blend solutions at elevated temperature. For all three polymers, the best plain devices were fabricated with a **P1–3**:$PC_{71}BM$ weight ratio of 1:3.5. Current density–voltage (*J–V*) curves of the optimized devices are shown in Fig. 4 and the device characteristics are summarized in Table 3. **P1** based devices exhibited a PCE of 2.60% with a V_{oc} of 0.76 V, a J_{sc} of 6.55 mA cm^{-2}, and an FF of 0.52. **P2** based devices demonstrated a PCE of 3.71% with a V_{oc} of 0.89, a J_{sc} of 6.80 mA cm^{-2}, and an FF of 0.61. **P3**:$PC_{71}BM$ based devices showed a PCE of 4.69% with a V_{oc} of 0.84 V, a J_{sc} of 8.51 mA cm^{-2}, and an FF of 0.65. The results clearly demonstrated that the enhancement of the solubility of polymers can improve the device performance. 1,8-Diiodooctane (DIO) is a good solvent for $PC_{71}BM$ but a poor solvent for conjugated polymers.[19] DIO (2.0% by volume) was therefore used as a processing additive to optimize the device performance,

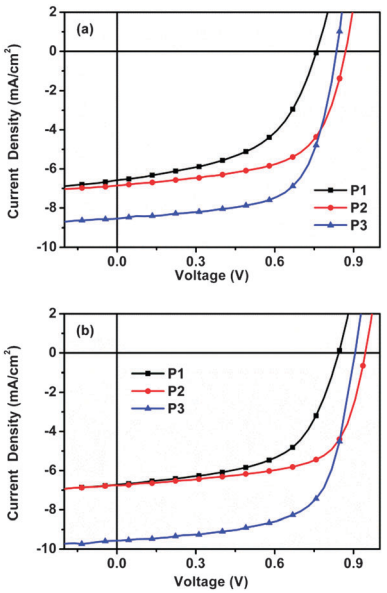

Fig. 4 *J–V* curves of **P1–3**:$PC_{71}BM$ based PSCs without (a) and with 2% DIO as an additive (b).

Table 3 Summary of the photovoltaic properties of **P1–4**:$PC_{71}BM$ under the illumination of AM 1.5G, 100 mW cm^{-2}

The active layer	DIO	V_{oc} (V)	J_{sc} (mA cm^{-2})	FF	PCE (best/average)	Thickness (nm)
P1:$PC_{71}BM$	No	0.76	6.55	0.52	2.60/2.34	98
	2%	0.86	6.76	0.58	3.34/2.90	108
P2:$PC_{71}BM$	No	0.89	6.80	0.61	3.71/3.68	105
	2%	0.93	6.80	0.65	4.12/4.06	115
P3:$PC_{71}BM$	No	0.84	8.51	0.65	4.69/4.63	117
	2%	0.91	9.49	0.66	5.71/5.60	115
P4:$PC_{71}BM$[a]	No	0.85	7.36	0.57	4.20	—

[a] Reference from literature.[19]

and the results are shown in Table 3. After adding DIO, all devices exhibited improved photovoltaic performance with V_{oc} increasing from 0.76 to 0.86 V for **P1**, from 0.89 to 0.93 V for **P2**, and from 0.84 to 0.91 V for **P3**. After adding DIO, the J_{sc} and FF values also slightly increased. The significant enhancement of V_{oc} indicated that the charge recombination in the devices is reduced and the enhancement of the FF value should be ascribed to the decreasing of series resistance for the devices.[27,28] To understand why using DIO as an additive can improve the device performance, the morphology of active layers was investigated by atomic force microscopy (AFM), the transport properties of active layers were investigated by the space-charge limited current (SCLC) method, and the elemental composition of the top and bottom surface of active layers was investigated by XPS (*vide infra*). These investigations demonstrated that the enhancement of device performance is mainly due to the optimized blend morphology and the improvement of vertical phase separation, namely the formation of a polymer rich bottom surface of the active layer, which are beneficial for the reducing of charge recombination and collecting of the charges by the electrode.[27,29] Our investigations have demonstrated that the use of a fluorinated carbazole unit

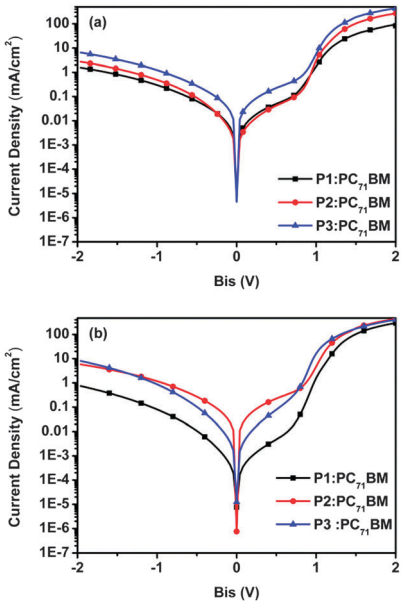

Fig. 5 Series resistor of devices based on **P1–3**:$PC_{71}BM$ as cast (a) and with 2% DIO as an additive (b).

as a donor unit has a positive effect for the photovoltaic performance.

R_s is an important factor that determines the FF value of photovoltaic devices, it has been demonstrated by many researchers that the reduction of R_s usually results in higher FF.[29] To elucidate what caused the improvement of FF value, we measured the R_s of devices. As shown in Fig. 5, R_s values were calculated from the inverse slope of dark *J–V* curves at a voltage of 1.0 V to be 53.25 Ω cm^{-2}, 21.06 Ω cm^{-2} and 10.48 Ω cm^{-2} for **P1**, **P2**, and **P3** based plain devices, respectively. As expected, the reduction of R_s resulted in an enhancement of the FF value. After adding DIO, the R_s values for **P1**, **P2**, and **P3** based devices were decreased to 46.91 Ω cm^{-2}, 14.59 Ω cm^{-2}, and 5.40 Ω cm^{-2}, respectively, which are consistent with the increasing of FF obtained from *J–V* measurements. This reducing could be ascribed to the optimized morphology by extending the side chain and using DIO as an additive (*vide infra*). These data are summarized in Table 4.

To examine the veracity of J_{sc}, external quantum efficiencies (EQEs) of devices fabricated without and with 2.0% DIO were measured. As shown in Fig. 6, all devices showed a broad EQE response from 350 to 700 nm. For plain devices, the EQE maximum reached 31% at 500 nm for **P1**, 44% at 542 nm for **P2**, and 53% at 467 nm for **P3**. By increasing the volume of side chains, namely the solubility of polymers, the EQE value increased. After adding 2.0% DIO as an additive, for three polymers EQE values only slightly increased. The integration of EQE curves afforded similar J_{sc} values to the *J–V* measurement, indicating that the J_{sc} values obtained from *J–V* measurements are reliable.

Transport properties

High efficiency PSCs require that the active layers are of balanced electron and hole mobility. Higher hole mobility is

Table 4 XPS surface element composition and series resistor of devices based on **P1–3**:$PC_{71}BM$

		Top		Bottom		
Devices	DIO	S (%)	C (%)	S (%)	C (%)	R_s (Ω cm^{-2})
P1:$PC_{71}BM$	No	2.06	88.51	6.43	66.09	53.25
	2%	2.22	88.44	6.50	65.37	46.91
P2:$PC_{71}BM$	No	1.47	90.02	5.98	67.89	21.06
	2%	2.06	88.51	6.04	67.76	14.59
P3:$PC_{71}BM$	No	1.17	91.14	5.48	67.97	10.48
	2%	1.32	90.55	5.64	67.77	5.40

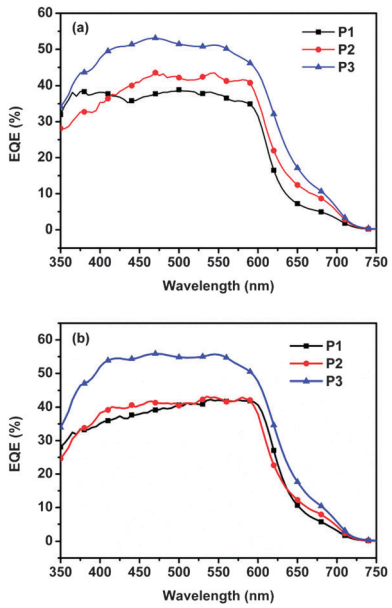

Fig. 6 EQE of **P1–3**:$PC_{71}BM$ based devices as cast (a) and with 2% DIO as an additive (b).

beneficial for achieving higher J_{sc} and FF. Hole mobilities (μ_h) of **P1–3**:$PC_{71}BM$ (1 : 3.5) blend films were measured by the space-charge limited current (SCLC) method. Hole-only devices with a structure of ITO/PEDOT:PSS (30 nm)/**P1–3**:$PC_{71}BM$/Au (100 nm) were fabricated. Dark *J–V* curves were fitted by using the Mott–Gurney equation: $J = 9\varepsilon_o\varepsilon_r\mu V^2/8L^3$, where J is the space charge limited current, ε_o is the vacuum permittivity, ε_r is the permittivity of the active layer, μ is the hole mobility, and L is the thickness of the active layer. As shown in Fig. S4 (ESI†), μ_h values of **P1**:$PC_{71}BM$, **P2**:$PC_{71}BM$, and **P3**:$PC_{71}BM$ based plain devices were calculated to be 1.1×10^{-6}, 3.3×10^{-5}, and 9.3×10^{-5} cm^2 V^{-1} s^{-1} respectively. The enhancement of hole mobility with increasing the volume of side chains should be ascribed to the better film morphology and lower R_s (*vide supra*). After adding 2.0% DIO, μ_h values of **P1**, **P2** and **P3** based devices were enhanced to 1.6×10^{-5}, 3.4×10^{-5}, and 1.1×10^{-4} cm^2 V^{-1} s^{-1}, respectively.

XPS measurement

The vertical distribution of the donor and acceptor materials in the active layer is very crucial for the performance of devices. Elemental compositions of the top (close to LiF layer) and

bottom (close to PEDOT:PSS layer) surfaces of the active layer in a depth of a few nanometers were therefore investigated by XPS. The top surface XPS experiment was conducted with the blend film on a glass substrate, and the bottom surface XPS experiment was conducted with a blend film which was spin-coated onto the PEDOT:PSS surface, floated on the surface of the pure water surface, and transferred onto a silicon substrate with the buried surface upward. The elemental compositions of sulfur (S) and carbon (C) at the top and bottom surfaces are summarized in Table 4. Because XPS is not a quantitative analysis method, these data could be used for semi-quantitative analysis of the distribution of two components.[12,30] XPS results showed that the content of S element at the bottom surface is much higher than that at the top surface, indicating that the blend films are of a vertical phase separation with a $PC_{71}BM$-rich top surface and a polymer-rich bottom surface. Such a vertical phase separation is beneficial to achieve high performance for conventional polymer solar cells. The formation of vertical phase separation is probably due to the following reasons. The polymers exhibit poorer solubility in DCB than $PC_{71}BM$ and they are prone to precipitate before the liquid–liquid phase separation occurs. Due to the centrifugation effect during spin-coating, the polymer precipitates could probably submerge to the bottom, the $PC_{71}BM$-rich DCB solution could be at the surface of the active layer, and finally the drying of the blend film leads to a vertical phase separation with a $PC_{71}BM$-rich top surface and a polymer-rich bottom surface. Since DIO is a good solvent for $PC_{71}BM$ and a poor solvent for the polymers, the use of 2.0% DIO as an additive will further promote the process of precipitation and retard the drying process of films.[12] As confirmed by the XPS results, the contents of the S element further increased, which are close to that of pure polymers after using 2.0% DIO as an additive. Compared with the corresponding active layers spin coated without using DIO, the polymer content at the top surface also slightly increased after the addition of DIO, similar to the literature results.[12] The reason for that is unclear at present time. Increasing the ohmic contact between the active layer and the electrode could be beneficial for the reducing of R_s and induce lower charge combination, which could lead to higher V_{oc}.[31–33] Such a vertical phase separation with almost a pure polymer thin layer at the bottom surface of the active layer was also beneficial for lowering the R_s and reducing the charge recombination at the bottom surface of the active layer.[34]

Film morphology

Film morphology of **P1–3**:$PC_{71}BM$ blend films spin coated from DCB solutions without and with 2% DIO as a processing additive is investigated by AFM in the tapping mode. As shown in Fig. 7, the **P1**:$PC_{71}BM$ films spin coated from DCB solution exhibited a rather rough surface with a root-mean-square (RMS) roughness value of 14.5 nm. Upon increasing the volume of flexible side chains, RMS values of **P2** and **P3** based blend films spin coated from DCB solutions were reduced to 7.24 nm and 3.41 nm, respectively. As indicated before, the solubility of **P2** and **P3** is gradually improved with the presence of elongated flexible side chains. The solubility of **P1–3** in DCB is poorer than that of $PC_{71}BM$. Therefore, we predict that the polymers

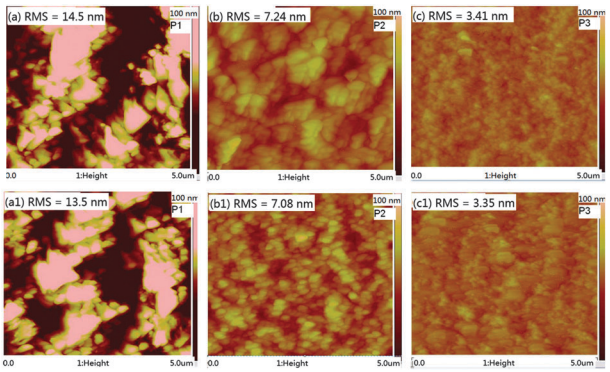

Fig. 7 AFM height images (5 μm × 5 μm) of **P1–3**:$PC_{71}BM$ blend films spin-coated from DCB solutions without (a–c) and with 2.0% DIO (a1–c1).

can precipitate first in solutions after spin-coating the hot blending solution onto the cold substrate before the film drying. The film drying procedure could be a liquid–solid mechanism. Due to the extremely poor solubility of **P1** in DCB at room temperature, **P1** is prone to form rough film morphology due to the solid–liquid phase separation.[17] **P3** exhibited the best solubility among these three polymers, as observed by AFM experiments, the film morphology of the **P3** based active layer is more uniform. **P2** exhibits medium solubility, and the domain size formed by **P2** is also of the medium size. After adding 2% DIO as an additive, the RMS roughness values of **P1–3** based blend films were slightly decreased, which demonstrated that DIO could optimize the film morphology. Smother morphology usually indicates phase separation on a smaller scale, which would be beneficial for the reducing of charge recombination.[35] The relatively low V_{oc} of **P1** based devices could be ascribed to the charge recombination caused by big domain sizes in the blend films. The RMS roughness values of **P1–3** based devices all decreased after adding 2% DIO into the active layer, demonstrating that DIO could optimize the morphology of devices and afford a more donor–acceptor interface, which would be beneficial to reduce the charge recombination and lead to higher V_{oc}.[36] Due to the domain size formed by liquid–solid phase separation became smaller, **P3**:$PC_{71}BM$ based PSCs gave the highest power conversion efficiency of 5.71% among these three polymers.

Conclusions

In summary, a series of new conjugated polymers (**P1–P3**) with 3,6-difluorocarbazole as a donor unit and benzoxadiazole as an acceptor unit were synthesized and used as donor materials for PSCs. These polymers exhibited poorer solubility than $PC_{71}BM$ in DCB. Among them, **P1** exhibited the poorest solubility, leading to the formation of large polymer domains due to the liquid–solid phase separation in the drying of blend films. By gradually extending the side chains for **P2** and **P3**, the solubility of polymers was increased, and the root mean square (rms) roughness values of blend films and the domain size of polymers decreased. Meanwhile, the hole mobility and series resistance

value were increased and decreased, respectively, which were beneficial to achieve higher PCE. For all polymers, using DIO as a solvent additive, series resistance values of devices were further reduced and hole mobility was slightly increased. XPS experiments also demonstrated for all polymers at the bottom surface of active layers processed with DIO as an additive became more polymer-rich, which is beneficial for the hole injection into the electrode. Using DIO could also optimize the film morphology, decrease the domain size, lower the R_s value, and enhance the fluorescence quenching efficiency, which would be beneficial for reducing charge combination, leading to higher V_{oc}. After optimization, PSCs based on **P3** finally gave the best PCE of 5.71%. Compared with the non-fluorinated polymer, fluorinated polymers exhibited lower HOMO levels. V_{oc}, J_{sc} and FF were all improved to furnish higher PCE. These preliminary results also demonstrated that the introduction of fluorine atoms at the donor unit is an effective way to achieve higher PCE.

Experimental part

2,7-Dibromo-9-(2-decyltetradecyl)-3,6-difluoro-9*H*-carbazole (2b)

A mixture of compound **1** (3.61 g, 10.0 mmol), NaH (60% in oil) (0.60 g, 15.0 mmol), 11-(bromomethyl)tricosane (5.01 g, 12.0 mmol) and DMF (50 mL) was stirred at 60 °C overnight under a nitrogen atmosphere. After removal of the solvent under reduced pressure, the residue was partitioned between water (200 mL) and dichloromethane (DCM, 50 mL). The organic layer was separated; the aqueous layer was extracted with DCM (50 mL × 3); and the combined organic layers were washed with brine (50 mL × 3), dried over anhydrous $MgSO_4$, and evaporated to dryness. The residue was further purified by chromatography on the silica gel with petroleum ether as an eluent to yield **2b** (5.72 g, 82%) as a colorless oil. ^{1}H NMR (400 MHz, $CDCl_3$): δ (ppm) 7.71–7.73 (d, J = 8.4 Hz, 2H), 7.51–7.52 (d, J = 5.6 Hz, 2H), 4.04–4.06 (d, J = 7.6 Hz, 2H), 2.05 (s, 1H), 0.86–1.25 (m, 47H). ^{13}C NMR (100 MHz, $CDCl_3$): δ (ppm) 141.81, 122.48, 121.38, 121.21, 119.63, 112.29, 47.83, 37.56, 35.49, 33.27, 31.92, 31.86, 31.77, 31.65, 29.89, 29.58, 29.49, 29.26, 28.72, 28.01, 26.37, 26.35, 22.66, 22.63, 15.22, 14.12, 14.09. MALDI-TOF (m/z): M^+ calculated for $C_{36}H_{53}Br_2F_2N$, 697.62; found: 697.58.

9-(2-Decyltetradecyl)-3,6-difluoro-2,7-bis(4,4,5,5-tetramethyl-1,3,2-dioxaborolan-2-yl)-9*H*-carbazole (3b)

A mixture of compound **2b** (1.00 mmol), bis(pinacolato)diboron (0.61 g, 2.40 mmol), KOAc (0.30 g, 5.00 mmol), $PdCl_2$(dppf) (0.22 mg, 0.03 mmol), and DMF (10 mL) was stirred at 80 °C for 3 d under a nitrogen atmosphere. After cooling down to room temperature, water (200 mL) was added, the mixture was extracted with ethyl acetate (50 mL × 3), and the combined organic layers were washed with brine (50 mL × 3), dried over anhydrous $MgSO_4$, and evaporated to dryness. The residue was purified by chromatography on the silica gel eluting with petroleum ether/ethyl acetate (5 : 1, v/v) to yield **3b** (0.49 g, 62%) as a colorless oil. ^{1}H NMR (400 MHz, $CDCl_3$): δ (ppm) 8.21–8.22 (d, J = 4.0 Hz, 2H), 7.62–7.64 (d, J = 8.8 Hz, 2H), 3.88–3.90 (d, J = 7.6 Hz, 2H), 2.21 (s, 1H), 1.01–1.41 (m, 71H). ^{13}C NMR (100 MHz, $CDCl_3$): δ (ppm) 140.90, 125.00. 124.69, 119.90, 115.66, 111.71, 47.33, 37.66, 35.59, 33.29, 32.10, 31.89, 31.80, 31.67, 31.63, 29.92, 29.57, 29.53, 29.27, 28.55, 27.88, 26.52, 26.39, 26.32, 24.92, 22.67, 22.59, 15.44, 14.89, 14.11, 13.97. MALDI-TOF (m/z): M^+ calculated for $C_{48}H_{77}B_2F_2NO_4$, 791.75; found: 791.70.

General procedure for the preparation of P1–3

A mixture of **3** (0.30 mmol), compound **4** (0.30 mmol), $NaHCO_3$ (1.25 g, 9 mmol), THF (20 mL), toluene (7 mL), and H_2O (2 mL) was degassed before and after $Pd(PPh_3)_4$ (6.9 mg, 5.96 μmol) was added. The mixture was heated to reflux and stirred for 3 d under a N_2 atmosphere. Phenylboronic acid (10 mg) and bromobenzene (0.2 mL) were added successively at a time interval of 12 h to end-cap the bromo and boronic acid end groups, respectively. After cooling down to room temperature, water (100 mL) and chloroform (100 mL) were added. The organic layer was separated, washed with water (50 mL × 3), and concentrated by evaporation of most of the solvent. The residue was poured into a large amount of acetone, and the resulting precipitates were collected by filtration and washed with acetone. The crude product was dissolved in a large amount of hot chlorobenzene and filtrated. After the removal of most of the solvent, the resulted concentrated solution was precipitated into a large amount of acetone and the precipitates were collected by filtration and dried under vacuum.

P1. **3a** and **4a** were used to synthesize **P1** according to the procedure described above. **P1** was obtained as a dark-red solid (196 mg, 70%). ^{1}H NMR (400 MHz, 1,2-dichlorobenzene-d_4): δ (ppm) 8.92–9.08 (m, 2H), 7.94–8.00 (m, 6H), 4.45–4.51 (m, 6H), 1.03–2.40 (m, 62H). GPC (PS standards): M_w = 51.0 kg mol^{-1}, M_n = 20.1 kg mol^{-1}, and PDI = 2.53.

P2. **3a** and **4b** were used to synthesize **P2** according to the above described procedure. **P2** was obtained as a dark-red solid (245 mg, 78%). ^{1}H NMR (400 MHz, 1,2-dichlorobenzene-d_4): δ (ppm) 9.08 (m, 2H), 7.95–8.01 (m, 6H), 4.44–4.53 (m, 6H), 1.06–2.45 (m, 78H). GPC (PS standards): M_w = 58.1 kg mol^{-1}, M_n = 22.1 kg mol^{-1}, and PDI = 2.63.

P3. **3b** and **4b** were used to synthesize **P3** according to the procedure described above. **P3** was obtained as a dark-red solid (282 mg, 81%). ^{1}H NMR (400 MHz, 1,2-dichlorobenzene-d_4): δ (ppm) 8.78–8.94 (m, 2H), 7.80–7.86 (m, 6H), 4.31–4.37 (m, 6H), 0.89–2.26 (m, 94H). GPC (PS standards): M_w = 77.5 kg mol^{-1}, M_n = 31.9 kg mol^{-1}, and PDI = 2.43.

Acknowledgements

Financial support from the NSF of China (21161160443), the 973 Programs (2011CB935702), Program for Changjiang Scholars and Innovative Research Team in University and the Fundamental Research Funds for the Central Universities is gratefully acknowledged.

References

1 Y. Liang, Z. Xu, J. Xia, S. T. Tsai, Y. Wu, G. Li, C. Ray and L. Yu, *Adv. Mater.*, 2010, **22**, E135.
2 Z. He, C. Zhong, S. Su, M. Xu, H. Wu and Y. Cao, *Nat. Photonics*, 2012, **6**, 591.
3 X. Zhan and D. Zhu, *Polym. Chem.*, 2010, **1**, 409.
4 Z. He, B. Xiao, F. Liu, H. Wu, Y. Yang, S. Xiao, C. Wang, T. P. Russell and Y. Cao, *Nat. Photonics*, 2015, **9**, 174.
5 Y. Liu, J. Zhao, Z. Li, C. Mu, W. Ma, H. Hu, K. Jiang, H. Lin, H. Ade and H. Yan, *Nat. Commun.*, 2014, **5**, 5293.
6 S. H. Liao, H. J. Jhuo, P. N. Yeh, Y. S. Cheng, Y. L. Li, Y. H. Lee, S. Sharma and S. A. Chen, *Sci. Rep.*, 2014, **4**, 6813.
7 C. Liu, C. Yi, K. Wang, Y. Yang, R. S. Bhatta, M. Tsige, S. Xiao and X. Gong, *ACS Appl. Mater. Interfaces*, 2015, **7**, 4928.
8 S. Liu, P. You, J. Li, J. Li, C. S. Lee, B. S. Ong, C. Surya and Y. Feng, *Energy Environ. Sci.*, 2015, **8**, 1463.
9 H. L. Yip and A. K. Y. Jen, *Energy Environ. Sci.*, 2012, **5**, 5994.
10 J. J. van Franeker, M. Turbiez, W. Li, M. M. Wienk and R. A. J. Janssen, *Nat. Commun.*, 2015, **6**, 6229.
11 X. Guo, N. Zhou, S. J. Lou, J. Smith, D. B. Tice, J. W. Hennek, R. Ponce Ortiz, J. T. Lopez Navarrete, S. Li, J. Strzalka, L. X. Chen, R. P. H. Chang, A. Facchetti and T. J. Marks, *Nat. Photonics*, 2013, **7**, 825.
12 Z. Lu, B. Jiang, X. Zhang, A. Tang, L. Chen, C. Zhan and J. Yao, *Chem. Mater.*, 2014, **26**, 2907.
13 H. Y. Chen, J. Hou, S. Zhang, Y. Liang, G. Yang, Y. Yang, L. Yu, Y. Wu and G. Li, *Nat. Photonics*, 2009, **3**, 649.
14 H. Zhou, L. Yang, A. C. Stuart, S. C. Price, S. Liu and W. You, *Angew. Chem., Int. Ed.*, 2011, **50**, 2995.
15 Y. Liang, D. Feng, Y. Wu, S. T. Tsai, G. Li, C. Ray and L. Yu, *J. Am. Chem. Soc.*, 2009, **131**, 7792.
16 M. Zhang, X. Guo, S. Zhang and J. Hou, *Adv. Mater.*, 2014, **26**, 1118.
17 S. Shi, X. Xie, P. Jiang, S. Chen, L. Wang, M. Wang, H. Wang, X. Li, G. Yu and Y. Li, *Macromolecules*, 2013, **46**, 3358.
18 H. Chen, J. Peet, S. Hu, J. Azoulay, G. Bazan and M. Dadmun, *Adv. Funct. Mater.*, 2014, **24**, 140.
19 S. Kouijzer, J. J. Michels, M. van den Berg, V. S. Gevaerts, M. Turbiez, M. M. Wienk and R. A. J. Janssen, *J. Am. Chem. Soc.*, 2013, **135**, 12057.
20 H. Wei, Y. H. Chao, C. Kang, C. Li, H. Lu, X. Gong, H. Dong, W. Hu, C. S. Hsu and Z. Bo, *Macromol. Rapid Commun.*, 2015, **36**, 84.
21 B. Zhang, X. Hu, M. Wang, H. Xiao, X. Gong, W. Yang and Y. Cao, *New J. Chem.*, 2012, **36**, 2042.
22 J. Liu, Y. Shi and Y. Yang, *Adv. Funct. Mater.*, 2001, **11**, 420.
23 C. Ramsdale, J. Barker, A. Arias, J. MacKenzie, R. Friend and N. Greenham, *J. Appl. Phys.*, 2002, **92**, 4266.
24 J. Kim, J. S. Yeo, H. G. Jeong, J. M. Yun, Y. A. Kim and D. Y. Kim, *Sol. Energy Mater. Sol. Cells*, 2014, **125**, 253.
25 S. Yamamoto, A. Orimo, H. Ohkita, H. Benten and S. Ito, *Adv. Energy Mater.*, 2012, **2**, 229.
26 M. D. Perez, C. Borek, S. R. Forrest and M. E. Thompson, *J. Am. Chem. Soc.*, 2009, **131**, 9281.
27 K. Vandewal, K. Tvingstedt, A. Gadisa, O. Inganäs and J. V. Manca, *Nat. Mater.*, 2009, **8**, 904.
28 B. Qi and J. Wang, *Phys. Chem. Chem. Phys.*, 2013, **15**, 8972.
29 Q. Yang, J. Wang, X. Zhang, J. Zhang, Y. Fu and Z. Xie, *Sci. China: Chem.*, 2015, **2**, 309.
30 C. Bruner, F. Novoa, S. Dupont and R. Dauskardt, *ACS Appl. Mater. Interfaces*, 2014, **6**, 21474.
31 Z. A. Page, Y. Liu, V. V. Duzhko, T. P. Russell and T. Emrick, *Science*, 2014, **346**, 441.
32 V. Mihailetchi, P. Blom, J. Hummelen and M. Rispens, *J. Appl. Phys.*, 2003, **94**, 6849.
33 C. J. Brabec, A. Cravino, D. Meissner, N. S. Sariciftci, T. Fromherz, M. T. Rispens, L. Sanchez and J. C. Hummelen, *Adv. Funct. Mater.*, 2001, **11**, 374.
34 W. C. Tsoi, S. J. Spencer, L. Yang, A. M. Ballantyne, P. G. Nicholson, A. Turnbull, A. G. Shard, C. E. Murphy, D. D. Bradley and J. Nelson, *Macromolecules*, 2011, **44**, 2944.
35 A. Gadisa, M. Svensson, M. R. Andersson and O. Inganäs, *Appl. Phys. Lett.*, 2004, **84**, 1609.
36 K. Vandewal, A. Gadisa, W. D. Oosterbaan, S. Bertho, F. Banishoeib, I. Van Severen, L. Lutsen, T. J. Cleij, D. Vanderzande and J. V. Manca, *Adv. Funct. Mater.*, 2008, **18**, 2064.